AADE-20-FTCE-SPP-10

Controlling Water Blockage Using Surfactant Into Fracturing Fluid: Optimum Interfacial Tension and Wettability Criteria

Nur Wijaya and James J. Sheng, Texas Tech University

Abstract

It is widely known that the recovery of hydraulic fracturing fluids is severely poor. The unrecovered portion of the fracturing fluids is believed to imbibe into the shale formation and creates formation damage, called "water blockage." The water blockage serves as one of the main challenges in shale oil recovery, because it decreases the oil relative permeability and increases the amount of drawdown required to recover the oil. One of the solutions to mitigate the water blockage is by adding surfactant into the fracturing fluids, because of the surfactant's ability in reducing the oil-water interfacial tension (IFT) and altering the wettability around the damaged/ leak-off zone.

Because of the additional cost of procuring the surfactant into the basic fracturing fluids program, the optimum surfactant screening becomes a relevant and an important question. Therefore, the objective of this study is to numerically investigate the optimum surfactant criteria for hydraulic fracturing fluids application, in terms of the IFT and wettability properties. Previous studies attempted to propose the optimum surfactant criteria by testing different surfactant blends of different IFT and wettability properties. However, the different surfactant blends might demonstrate different physiochemical properties, such as surfactant adsorption and partitioning behavior. In other words, the experimental approach cannot objectively single out the effect of IFT and wettability, and thus leading to questionable experimental results.

Therefore, this study aims to propose the optimum surfactant criteria using a numerical approach. The numerical model is validated based on a successful history match with surfactant laboratory experimental data. Our numerical model indicates that in conventional reservoirs, the optimum surfactant criteria are ultralow-IFT surfactants. However, in tight reservoirs, the optimum surfactant criteria are not only surfactants with the ultralow IFT, but also with a minimum wettability alteration toward water-wet.

Introduction

Hydraulic fracturing has become an inevitable stimulation technique to allow economic production from shale oil reservoirs [1]. During the fracturing, a large volume of the fracturing fluids along with proppants is injected into the reservoirs to create complex fracture network. The different pumping schedules create a complex fracture network and proppant distribution [2]. However, despite the complex fracture network and proppant distribution, it is consistent that only a small fraction of the fluids is recovered during flowback. It is perceived that the unrecovered fluids imbibe into the matrix because of the high capillarity of the tight reservoirs and the high injection pressure applied. The imbibition leads to a liquid blockage at matrix-fracture interface, called "water blockage." The water blockage serves as one of the main challenges in shale oil recovery, because it decreases the oil relative permeability and increases the amount of drawdown required to recover the oil [3].

To remove the water blockage, field operators often decide to add surfactant into the fracturing fluids. Some other studies suggested injecting liquid or gas nitrogen to enhance the matrix permeability around fractures [4-5]. In fact, in addition to the surfactant, acid is often added to the fracturing fluids as well to etch the carbonate components of the shale for a better permeability near fractures [6-7]. Surfactant is a solution of surface acting agents, which consist of a hydrophobic tail and a polar hydrophilic head group [8]. The polar and non-polar head allow the surfactant to encapsulate the initially immiscible oil and water to an emulsion or miscible microemulsion phase. This solubilization behavior allows the surfactant to reduce the interfacial tension (IFT) between the water (i.e., fracturing fluids) and the oil (i.e., in-situ hydrocarbon). By reducing the IFT, the water blockage can be more easily recovered because a portion of the water blockage will be carried by the oil components that flow out of the matrix during the oil production period. Given the numerous options of the surfactant blends, some surfactants reduce the IFT moderately from an initial oil-water IFT of approximately 30 mN/m to a range of 0.1 to 10 mN/m, whereas others to an ultralow range (i.e., up to 0.001 mN/m). Another advantage of the surfactant is that it can alter the rock wettability. The wettability alteration phenomenon is related to a complex thermodynamic equilibrium between the surfactant molecules and the charged rock surface. Given the numerous options of the surfactant blends, some surfactants alter the rock wettability to more water-wet, while others to more oil-wet.

Previous lab and field studies have confirmed the benefits of adding surfactants into the fracturing fluid over water alone. For example, a series of spontaneous imbibition performed by Kim et al. (2016) [9] and Neog and Schechter (2016) [10]

demonstrated that all of their tested surfactants yield a higher oil recovery than fracturing water alone. In regards to mitigating the water blockage, lab experiments have also proven that surfactants achieved a higher regain of hydrocarbon permeability than fracturing water, even as high as 80% [8,11-14]. Similarly, as far as the field observation, the load recovery or flowback recovery from over 200 wells in Cotton Valley, Greater Green River, Piceance, San Juan, Uinta, and Vicksburg Basin treated with surfactants is 50 to 100% higher than the load recovery with fracturing water alone [15-16]. In fact, some field operators in the Appalachian, Barnett, and Fayetteville Basin observed an increase in the initial natural gas production rate from wells treated with surfactants [17-19].

Although the concept of adding the surfactant into the fracturing fluids is logically reasonable and proven in the field, it requires further studies, especially on the surfactant selection, because there are numerous surfactant blends manufactured. In terms of the IFT, the different blends can either reduce the IFT moderately or significantly. Similarly, in terms of the wettability, the different blends can either alter the rock wettability to more water-wet or oil-wet moderately or significantly. Furthermore, the procurement of surfactant into the fracturing fluids incurs additional costs over the basic fracturing fluid program. Therefore, the optimization of surfactant selection criteria becomes a relevant and an important question because the investment on the surfactant should result in an optimum removal of the water blockage.

Therefore, the objective of this study is to investigate the optimum surfactant criteria for the fracturing fluids application, solely in terms of the IFT and wettability properties. There have been studies that investigated the performance of adding the surfactant into the fracturing fluids in removing the water blockage. Most of these previous studies performed an experimental approach by testing different surfactant blends corresponding to different IFT values and wettability alteration properties. However, given the complex physiochemical properties of the surfactant, such an experimental approach (i.e., testing the different surfactant blends) could lead to misleading results, because the different surfactant blends might demonstrate significantly different thermodynamic properties, such as surfactant partitioning (because the surfactant can dissolve into both the oil and water phase) and surfactant adsorption (i.e., from the bulk liquid phase to the solid rock phase). Because the surfactant partitioning serves as one of the physical mechanism of the IFT reduction phenomenon, the surfactant partitioning must be treated as a control variable. Similarly, because the surfactant adsorption serves as one the physical mechanism of the wettability alteration phenomenon, the surfactant adsorption must be treated as another control variable.

Therefore, this study uses a numerical modeling approach, because it can objectively single out the effect of IFT reduction and wettability alteration, while completely controlling/ fixing the other surfactant physiochemical properties. To validate the numerical model, this study uses some data from previous surfactant laboratory experiments. In fact, the experimental data are quite comprehensive that the numerical model is built and developed more realistically. The experimental data range from water saturation profiles inside core samples obtained from a Computed Tomography (CT) scanner to pressure drop profiles throughout the coreflood experiments. Therefore, not only that the numerical model can objectively single out the effect of IFT reduction and wettability alteration, the numerical model is strongly validated by matching the numerical results with the myriad experimental results, all from a single model.

Methodology

Model Development

The numerical model is built in a compositional multiphase flow simulator [20], by modeling three different components: water, oil, and surfactant. We model only these three components, because the experiment from which we will obtain the experimental data only modeled these three components. In a compositional multiphase flow, the full set of governing equations generally includes mass conservation, chemical reaction equations, fugacity equalities, and other constraints. In this study, the fugacity equalities are replaced by tables of equilibrium ratios (i.e., K-values) in the water and oil phase for each component.

For paper comprehensiveness, this section presents the governing equations of the multiphase flow in porous media in the compositional approach. Let $\xi_{i\alpha}$ be the molar density of component i in phase α, with a dimension of moles per pore volume. If W_i is the molar mass of component i, with a dimension of mass of component i/ mole of component i, $\xi_{i\alpha}$ is related to the mass density $\rho_{i\alpha}$ by

$$\xi_{i\alpha} = \frac{\rho_{i\alpha}}{W_i}, \qquad \alpha = o, w. \tag{1}$$

The molar density of phase α is

$$\xi_\alpha = \sum_{i=1}^{N_{comp}} \xi_{i\alpha}, \qquad \alpha = o, w \tag{2}$$

where N_{comp} is the number of components (i.e., 3 in this study). Afterward, the mole fraction of component i in phase α is given by

$$X_{i\alpha} = \frac{\xi_{i\alpha}}{\xi_\alpha}, \qquad \alpha = o, w. \tag{3}$$

In general, the full set of governing equations for chemical-compositional modeling includes statements of mass conservation, chemical reaction equations, fugacity equalities, and other constraints. The general mass conservation equations for component i in fluid phases and solid species m are

$$\frac{\partial}{\partial t}\left(\sum_{\alpha=1}^{n_\alpha}(\phi\rho_\alpha S_\alpha X_{i\alpha})\right) + \nabla\cdot\mathbf{L} + q_i^W = \sum_{k=1}^{n_k} v_{ik} r_k + \sum_{q=1}^{n_q} v_{iq} r_q, \tag{4}$$

$$\frac{\partial C_m}{\partial t} = \sum_{k=1}^{n_k} v_{mk} r_k + \sum_{q=1}^{n_q} v_{mq} r_q, \tag{5}$$

where

$$\mathbf{L} = \sum_{\alpha=1}^{n_\alpha}(\rho_\alpha X_{i\alpha}\mathbf{u}_\alpha - \rho_\alpha\phi S_\alpha \mathbf{D}_{i\alpha}\nabla X_{i\alpha}), \tag{6}$$

where t is time, n_α is the number of fluid phases, ϕ is porosity, ρ_α is the density of fluid phase α, S_α is the saturation of phase α, $\mathbf{u}_\alpha$ is the Darcy velocity of phase α (defined below), $\mathbf{D}_{i\alpha}$ is the dispersion tensor for component i in fluid-phase α, q_i^W is the well rate of component i, C_m is solid species concentration, v_{ik} are the stoichiometric coefficients of

component i in kinetic reaction k, v_{iq} are the stoichiometric coefficients in equilibrium reaction q, r_k and r_q are the rates of kinetic reaction k and equilibrium reaction q, respectively, and n_k and n_q are the numbers of kinetic and equilibrium reactions, respectively. The Darcy velocity for phase α is given by

$$\mathbf{u}_\alpha = -\mathbf{k}\frac{k_{r\alpha}}{\mu_\alpha}(\nabla p_\alpha - \rho_\alpha g \nabla D), \qquad \alpha = 1, \dots, n_\alpha, \tag{7}$$

where $\mathbf{k}$ is the permeability tensor, $k_{r\alpha}$ is the relative permeability for phase α, μ_α is the velocity of phase α, p_α is the pressure of phase α, g is gravitational acceleration, and D is depth.

In this study, the model is also set to be one-dimensional, isothermal, and without dispersion. We assume that the solid grains are non-reacting to other phases. We also model two fluid phases only (i.e., oil and water), because the laboratory experimental results that we will use to validate the model only consist of oil and water. The solution is also simplified by assuming that equilibrium conditions exist for the partitioning of the components between the two phases modeled (i.e., oil and water) at given temperature and pressure conditions.

Given the simplifications, the conservation of mass equations for any component i present in the water phase can be expressed as

$$\frac{\partial}{\partial t}(\phi \rho_w S_w X_{iw}) + \nabla \cdot (\rho_w X_{iw} \mathbf{u}_w) = (R^i_{ow} - R^i_{wo}) + (R^i_{sw} - R^i_{ws}) + R^i_{source_w} - R^i_{sink_w}, \tag{8}$$

where R^i_{ow} is the mass transfer rate of component i from the oil phase to the water phase, R^i_{wo} is the mass transfer rate of component i from the water phase to the oil phase, R^i_{sw} is the mass transfer rate of component i from the solid phase to the water phase (i.e., desorption), R^i_{ws} is the mass transfer rate of component i from the water phase to the solid phase (i.e., adsorption), $R^i_{source_w}$ is the source term (positive) of mass of component i in the water phase, and R^i_{sink} is the sink term (negative) of mass of component i in the water phase. The last two terms are due to fluid injection or withdrawal, respectively. The summation of the equations for each component in the water phase would give the conservation of mass equation for the water phase. Similarly, the conservation of mass equations for any component i present in the oil phase can be expressed as

$$\frac{\partial}{\partial t}(\phi \rho_o S_o X_{io}) + \nabla \cdot (\rho_o X_{io} \mathbf{u}_o) = (R^i_{wo} - R^i_{ow}) + (R^i_{so} - R^i_{os}) + R^i_{source_o} - R^i_{sink_o}, \tag{9}$$

where similar symbols apply but the subscript o now refers to the oil phase.

After the governing equations of the multiphase flow in porous media are presented, this section presents the algorithms used particularly to numerically model the IFT reduction and wettability alteration phenomena due to the presence of surfactant in the model. Since the surfactant generally improves the relative permeability of each phase and decreases the capillary pressure, a number of different sets of saturation tables is required, corresponding to different wettability states and surfactant concentrations. To generate the relative permeability curves, our model uses Corey-type relative permeability models, which are given by (Brooks and Corey, 1964)

$$k_{rw} = k_{rw,endpoint}\left(\frac{S_w - S_{wirr}}{1 - S_{wirr} - S_{or}}\right)^{n_w} \tag{10}$$

$$k_{ro} = k_{ro,endpoint}\left(\frac{1 - S_w - S_{or}}{1 - S_{wirr} - S_{or}}\right)^{n_o} \tag{11}$$

where k_{rw} and k_{ro} are the water and oil relative permeability, respectively; $k_{rw,endpoint}$ and $k_{ro,endpoint}$ are the maximum water and oil relative permeability, respectively; S_w is the water saturation; S_{wirr} is the irreducible water saturation; S_{or} is the residual oil saturation; and n_w and n_o are the Corey's relative permeability exponent for water and oil, respectively.

Afterwards, to model the relative permeability improvement, capillary number (Equation (12)) is used as the interpolation parameter of the relative permeability and capillary pressure curves, using the following model [20]:

$$N_c = \frac{\mu v}{\sigma} \tag{12}$$

$$k^{IFT}_{rw,watwet} = (1 - \gamma)\, k^{low}_{rw,watwet} + \gamma\, k^{high}_{rw,watwet} \tag{13}$$

$$k^{IFT}_{ro,watwet} = (1 - \gamma)\, k^{low}_{ro,watwet} + \gamma\, k^{high}_{ro,watwet} \tag{14}$$

$$P^{IFT}_{c,watwet} = (1 - \gamma)\, P^{low}_{c,watwet} + \gamma\, P^{high}_{c,watwet} \tag{15}$$

where

$$\gamma = \frac{\log(N_c) - \log(N_c^{low})}{\log(N_c^{high}) - \log(N_c^{low})} \tag{16}$$

in which $k^{IFT}_{rw,watwet}$ is the k_{rw} of the water-wet rock after IFT reduction effect but before wettability alteration effect is incorporated, $k^{IFT}_{ro,watwet}$ is the k_{ro} of the water-wet rock after IFT reduction effect but before wettability alteration effect is incorporated, $P^{IFT}_{c,watwet}$ is the P_c of the water-wet rock after IFT reduction effect but before wettability alteration effect is incorporated, and γ is the interpolation parameter for the IFT reduction. The superscript low and high indicate the parameter value at the low and high capillary number, respectively. Similar algorithm is applied to the oil-wet saturation table, so that these terms will also be computed: $k^{IFT}_{rw,oilwet}$, $k^{IFT}_{ro,oilwet}$, and $P^{IFT}_{c,oilwet}$.

After the effect of IFT reduction is calculated, the effect of wettability alteration is subsequently calculated. The wettability alteration is modeled through surfactant adsorption phenomenon. Our model uses the Langmuir adsorption model, which is given by

$$\delta = \frac{a_s C_s}{1 + b_s C_s} \tag{17}$$

where δ is the mole fraction of surfactant component in the adsorbed phase, C_s is the mole fraction of surfactant in the liquid phase, a_s is the first parameter in the Langmuir isotherm, and b_s is the second parameter in the Langmuir isotherm.

This mole fraction of surfactant component in the adsorbed phase (δ) is later used to calculate the interpolation parameter between water-wet and oil-wet saturation table (i.e., wettability alteration). Therefore, after the relative permeability and capillary pressure values due to the IFT reduction are computed, the following algorithms are subsequently used to calculate the final relative permeability and capillary pressure after both the IFT reduction and wettability alteration effects are incorporated [20]:

$$k_{rw} = k_{rw,watwet}^{IFT} + \omega\left(k_{rw,oilwet}^{IFT} - k_{rw,watwet}^{IFT}\right) \quad (18)$$

$$k_{ro} = k_{ro,watwet}^{IFT} + \omega\left(k_{ro,oilwet}^{IFT} - k_{ro,watwet}^{IFT}\right) \quad (19)$$

$$P_c = P_{c,watwet}^{IFT} + \omega\left(P_{c,oilwet}^{IFT} - P_{c,watwet}^{IFT}\right) \quad (20)$$

where

$$\omega = \left(\frac{\frac{1}{\delta-\delta_{watwet}+\varepsilon}-\frac{1}{\varepsilon}}{\frac{1}{\delta_{oilwet}-\delta_{watwet}+\varepsilon}-\frac{1}{\varepsilon}}\right)^{\tau} \quad (21)$$

in which ω is the interpolation parameter for the wettability alteration, δ_{watwet} is the mole fraction of surfactant component in the adsorbed phase in completely water-wet rock, δ_{oilwet} is the mole fraction of surfactant component in the adsorbed phase in completely oil-wet rock, ε is the first weighting factor, and τ is the second weighting factor which will create a tendency behavior within the interpolation. In short, after the effect of IFT reduction on the saturation tables is calculated using Equations (13) to (16), the effect of wettability alteration is subsequently calculated using Equations (17) to (21).

Model Validation

The numerical model is validated based on previous surfactant coreflood experimental data [13]. In their experiment, the fracturing fluid is injected into one side of the core sample to simulate the invasion/ leak-off of the fracturing fluids into the formation. After 80-min injection, oil (pentane) is injected into the other side of the core sample to simulate the flowback process and the extended oil production. The experiment simulated two types of fracturing fluids: deionized (DI) water and surfactant solution. The entire coreflood setup is positioned inside a Computed Tomography (CT) scanner (Fig. 1). Therefore, the evolution of the water saturation distribution or profile inside the core sample was continuously monitored and acquired. In other words, the experiment provided multiple water saturation profiles corresponding to different time slices during the invasion and flowback stage (Fig. 2). The color numbers obtained from the CT scanner are then calibrated to convert the colorful data into numerical data, showing the actual water saturation profiles in two dimensions (Fig. 3). These water saturation profiles are later used as some of the parameters that the numerical model must closely reproduce for the model validation purposes. It is also important to note that the experiment was conducted at a room temperature. Therefore, the experiment does not very closely simulate the temperature effect on the core sample permeability required to remove the water blockage in the subsurface reservoir [21].

Using the algorithms presented in the previous section, the numerical model is successfully validated by history matching the experimental data, ranging from the water saturation profiles for the DI-water injection (Fig. 4), the water saturation profiles for the surfactant injection (Fig. 5), and the pressure drop for both the DI-water and surfactant injection during both the invasion and flowback stage (Fig. 6) [22].

Fig. 1. Coreflood experiment conducted inside the CT scanner [13].

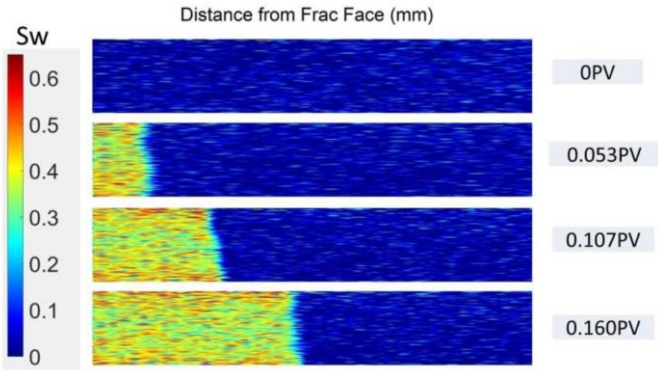

Fig. 2. Raw data of the water saturation profiles obtained from the CT scanner [13].

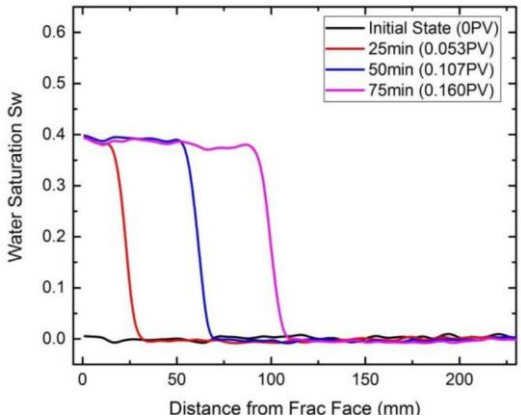

Fig. 3. Processed data of the water saturation profiles from the experiment [13].

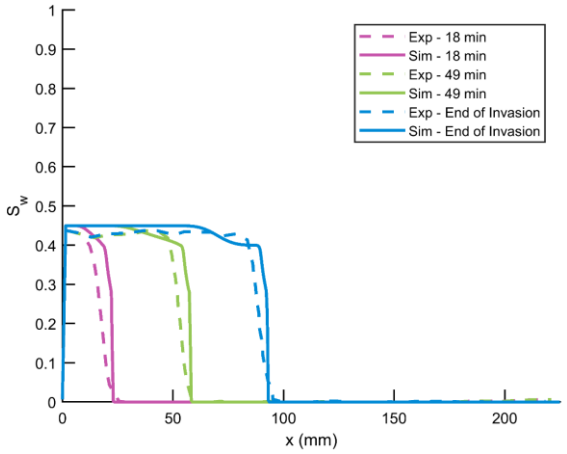

Fig. 4. Model validation on water saturation profiles for DI-water injection: experiment vs. model (simulation).

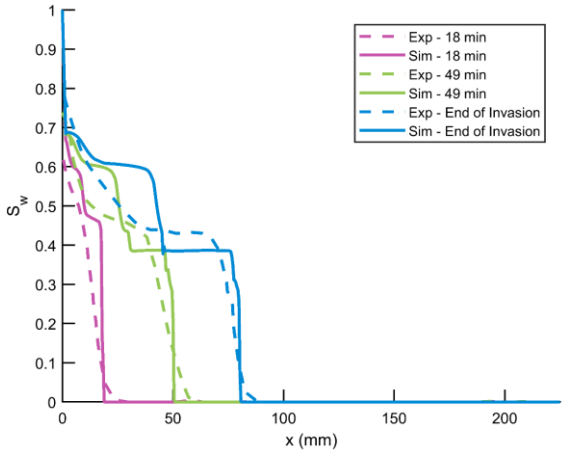

Fig. 5. Model validation on water saturation profiles for surfactant injection: experiment vs. model (simulation).

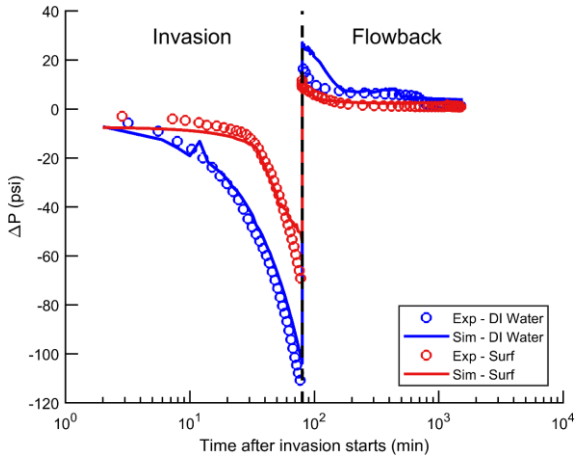

Fig. 6. Model validation on pressure drop data for both DI-water injection (blue) and surfactant injection (red) for both the invasion and flowback stage: experiment vs. model (simulation).

Results and Discussion: Base Model

After the numerical model is strongly validated, this section presents the sensitivity analysis of the combined effect of IFT and wettability on the efficiency of water blockage removal. As far as the IFT, we investigate a wide range of IFT, starting from high IFT (20 mN/m) to ultralow IFT (0.001 mN/m). Meanwhile, as far as the wettability alteration, we investigate only surfactants that alter the rock wettability to more water-wet, because the effect of the oil-wetting surfactant has previously been investigated [23]. To model the wettability alteration effect, at least two sets of relative permeability and capillary pressure curves must be provided: one corresponding to the initial state (i.e., before the surfactant adsorption), while the other one to the altered state (i.e., after the surfactant adsorption). Fig. 7 presents the relative permeability curves before and after the wettability alteration, while Fig. 8 shows the capillary pressure curves before and after the wettability alteration.

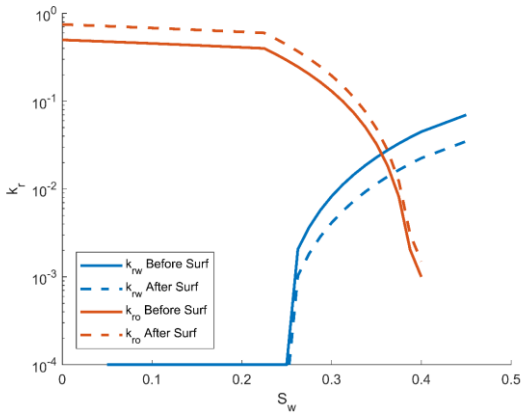

Fig. 7. Relative permeability curves before and after the wettability alteration due to the adsorption of water-wetting surfactant.

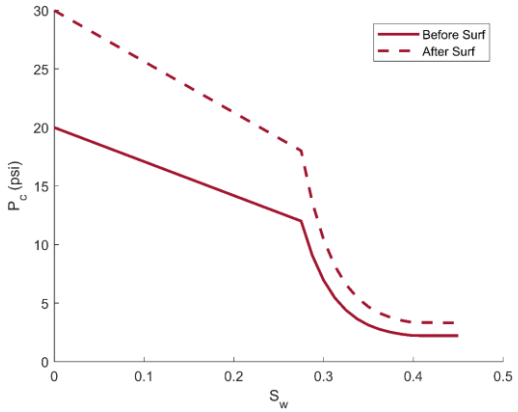

Fig. 8. Capillary pressure curves before and after the wettability alteration due to the adsorption of water-wetting surfactant.

The relative permeability and capillary pressure curves at the altered state can vary widely depending on the wettability alteration capacity of each surfactant blend. Therefore, because of the uncertainty of the extent of the wettability alteration, this study simulates different wettability alteration extents from weak to strong. Because the wettability alteration is modeled based on the amount of surfactant adsorbed, Fig. 9 illustrates the different amounts of surfactant adsorbed, corresponding to different wettability alteration extents.

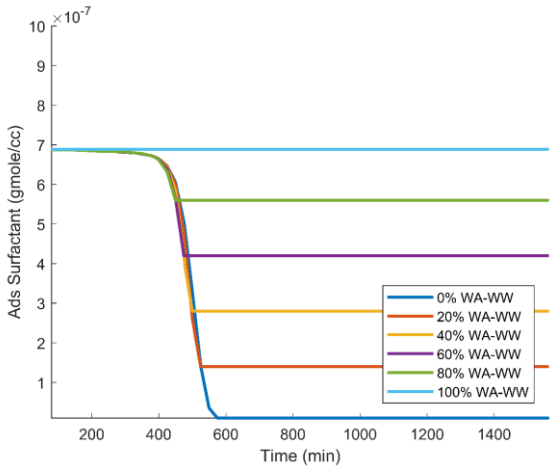

Fig. 9. Modeling approach for different wettability alteration extents.

In this study, the objective function used to quantify the efficiency of the water blockage removal is the oil relative permeability (k_{ro}) during the flowback stage, which is given by

$$k_{ro} = \frac{q_o \mu_o L}{kA\Delta P} \quad (22)$$

where q_o is the oil volumetric flow rate during the flowback stage, μ_o is the oil viscosity, L is the length of the core sample, k is the absolute permeability of the core sample, A is the cross-sectional area of the core sample perpendicular to the flow, and ΔP is the pressure drop across the core during the flowback stage. The oil relative permeability is considered as a suitable objective function because this parameter normalizes the flowback rate by the pressure drop [24].

During the IFT and wettability optimization, the oil relative permeability demonstrates a time-dependent phenomenon, which causes the oil relative permeability to fluctuate with time [22]. This occurs because during flowback, some of the surfactants are desorbed from the rock surface, which thus changes the wettability alteration extent. Some of the surfactants are also recovered from the core sample during the flowback, which causes the IFT in the damaged zone to gradually revert to the initial value. Therefore, Fig. 10 shows three separate heat maps, which correspond to the early-, intermediate-, and late-time region, respectively. The early-time region refers to a period in which the IFT in the damaged zone is still the target IFT. The intermediate-time region refers to a period in which the IFT in the damaged zone is gradually increased to the initial oil-water IFT value. Lastly, the late-time region refers to a period in which the IFT in the damaged zone has returned to the initial oil-water IFT value. In Fig. 10, the x-axis corresponds to the wettability alteration extents, whereas the y-axis corresponds to the target IFT, shown in a logarithmic scale to accommodate the wide range of the IFT.

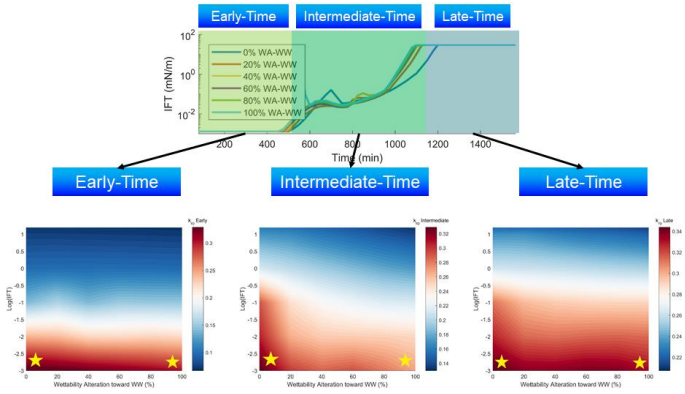

Fig. 10. Optimum IFT and wettability criteria to mitigate the water blockage in conventional rocks (base model).

Fig. 10 shows that in the base model, the optimum surfactant criteria to mitigate the water blockage are mainly ultralow-IFT surfactants, illustrated by the yellow star located at the bottom of each of the heat maps, spread out from 0 to 100% wettability alteration. This numerical result can be physically explained by the fact that when the IFT is ultralow, the relative permeability curves are significantly improved that both water and oil can flow out of the imbibed zone easily. In fact, when the IFT is ultralow, the capillary pressure at the imbibed zone is virtually zero, and hence there is no capillary discontinuity at the matrix-fracture interface, which will allow an easier removal of the water blockage.

Results and Discussion: Tight Model

However, the base model demonstrates permeability in the range of millidarcy which could be considered as conventional rocks. To more closely simulate the fracturing operation in the field, the rock permeability should significantly be lower, such as within a nanodarcy range. Therefore, we perform a permeability upscaling using J-function to change the permeability from the base value obtained from the lab experiment (3.69 mD) to the typical shale core permeability (500 nD) [25-26]. The J-function is given by

$$J(S_w) = \frac{CP_c}{\sigma \cos(\theta)} \sqrt{\frac{k}{\varphi}} \quad (23)$$

where $J(S_w)$ is the Leverett J-function which is a function of water saturation, C is the unit conversion factor, P_c is the capillary pressure, σ is the interfacial tension, θ is the contact angle, k is the permeability, and φ is the porosity. In the tight model, the invasion duration is changed from 80 to 180 min, while the flowback duration is extended to two weeks to mimic the flowback operations after hydraulic fracturing in the field [27]. The surfactant properties are kept the same as in the base model (i.e., altering the wettability to more water-wet). The

same workflow of IFT and wettability optimization is applied in the tight model.

Fig. 11 shows that in the tight model, the optimum surfactant criteria to mitigate the water blockage are not only ultralow-IFT surfactants, but also minimum wettability alteration to water-wet, illustrated by the yellow star located at the bottom left corner of the late-time region heat map. This numerical result can be physically explained by the fact that as the permeability is in the nanodarcy range, the capillary pressure can reach as high as thousands of psi. When the damaged zone is altered to more water-wet, the capillary pressure will be even higher. A higher (more positive) capillary pressure means that there will be a stronger suction force that causes the water blockage to remain trapped more permanently at the matrix-fracture interface.

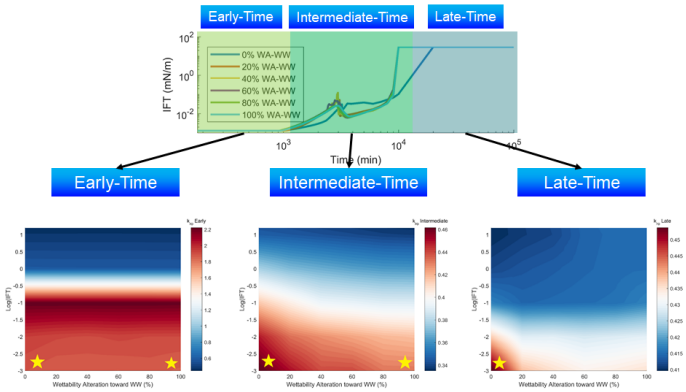

Fig. 11. Optimum IFT and wettability criteria to mitigate the water blockage in unconventional rocks (tight model).

Experimental Verification

To support our modeling results, the experiments performed by Liang et al. (2017) [13] and Tangirala and Sheng (2019) [28] are discussed. Unlike in the other surfactant experiments which simply performed imbibition tests, these two particular experiments specifically inject different surfactant-invasion fluids into the core samples first. Then, a flowback process is carried out to measure the regained oil relative permeability, to compare which surfactant types mitigate the water blockage more effectively. As illustrated in Fig. 12, Liang et al. (2017) [13] showed that in a 3.69-mD core, ultralow-IFT surfactants (up to 0.0013 mN/m) ("Good") removes the water blockage better than moderate- or high-IFT surfactants (up to 23 mN/m) ("Bad"). This helps validate our modeling results that in the base model, given the conventional-range permeability, ultralow IFT is the optimum IFT criterion.

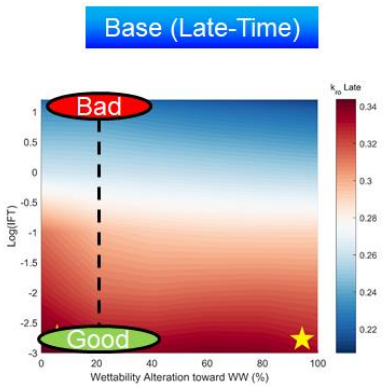

Fig. 12. Experimental verification for modeling results on the optimum surfactant criteria to mitigate the water blockage in conventional rocks (base model).

On the other hand, Tangirala and Sheng (2019) [28] compared both oil-wetting and water-wetting surfactants at a relatively the same IFT value of 0.5 mN/m into a tight core sample (i.e., 0.1 mD). Their results showed that in the tight core, as illustrated in Fig. 13, oil-wetting surfactants ("Good) remove the water blockage better than water-wetting surfactants ("Bad"). This helps further validate our modeling results that in the tight model, oil-wetting surfactants are the optimum wettability criterion. Therefore, not only that the modeling results have been supported by experimental data, the modeling results also enrich the current literature by carefully predicting the performance of the water-wetting surfactants at a much larger range of IFT and wettability alteration extent than what the currently-available flowback surfactant experimental data have provided.

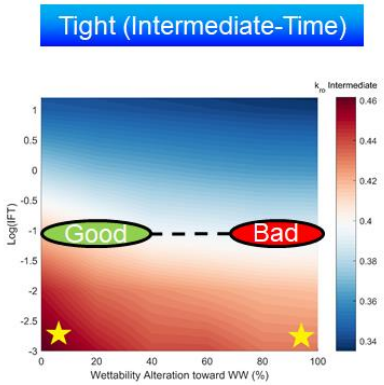

Fig. 13. Experimental verification for modeling results on the optimum surfactant criteria to mitigate the water blockage in unconventional rocks (tight model).

Conclusions

This study focuses on numerically optimizing the surfactant criteria for water blockage control applications, primarily in terms of the interfacial tension and wettability alteration properties. The numerical modeling study is carried out because the experimental study cannot objectively investigate the effect of the interfacial tension and wettability alteration, because the experimental approach tested different surfactant blends which

could correspond to different surfactant partitioning and adsorption as well. The numerical model is validated through a reasonable history match with laboratory experimental data on surfactant coreflood. The following conclusions can be drawn from the presented weork.

- The optimum surfactant criteria for water blockage control depend on the level of capillarity of the rocks.
- In conventional rocks, the optimum criteria are to select surfactants that offer ultralow IFT (even as low as 0.001 mN/m).
- In unconventional or tight rocks, the optimum criteria are to select surfactants that not only offer ultralow IFT, but also a minimum wettability alteration to water-wet.

This study focuses on the surfactant performance solely in removing the water blockage rather than its effect on the ultimate oil recovery. Therefore, investigating whether simply removing the water blockage could lead to an improved oil recovery is our future work.

Acknowledgments

The authors would like to acknowledge Computer Modeling Group Limited for the CMG reservoir simulation software. The authors also acknowledge the High Performance Computing Center (HPCC) at Texas Tech University at Lubbock for providing the high performance computing resources.

References

1. Mansour, A. G., Khalil, R., Gamadi, T. 2017. Compositional Simulation Evaluation of Miscible Gas Injection Performance in Tight Oil Formation. In: SPE Western Regional Meeting. Society of Petroleum Engineers. SPE-185680-MS.
2. Altawati, F., Ramezanian, M., Saoyleh, Soliman, M., H., Emadi, H., 2020. The Effect of Proppant Ramping and Hydraulic Fracturing for High-Permeable Oil and Low-Permeable Gas Zones. In: 54th U.S. Rock Mechanics/ Geomechanics Symposium. American Rock Mechanics Association. ARMA 20-1055.
3. Altawati, F., Sheng, J. J., Emadi., H., 2020. Investigating Effects of Water on Shale Oil Formations by Using Cyclic Gas Injection Technique-An Experimental Study. In: 54th U.S. Rock Mechanics/ Geomechanics Symposium. American Rock Mechanics Association. ARMA 20-1054.
4. Altawati, F., Ramezanian, M., Khalil, R., Emadi, H., 2020. Effect of Thermal Shock Treatments on Permeability and Dynamic Elastic Properties of Wolfcamp Formation – An Experimental Study. In: 54th U.S. Rock Mechanics/ Geomechanics Symposium. American Rock Mechanics Association. ARMA 20-1303.
5. Khalil, R., Emadi, H., Heinze, L.R., 2020. An Experimental Study Analyzing Effects of Cryogenic Treatments on Porosity, Permeability, and Dynamic Elastic Properties of Marcellus Formation Core Samples. In: 54th U.S. Rock Mechanics/ Geomechanics Symposium. American Rock Mechanics Association. ARMA 20-1110.
6. Khalil, R. E., Mansour, A., Gamadi, T., 2017. An Experimental Study of Acid Matrix Treatment Performance on Shale Core Samples. In: SPE Liquids-Rich Basins Conference-North America. Society of Petroleum Engineers. SPE-187478-MS.
7. Khalil, R., Emadi, H., Gamadi, T., 2020. An Experimental Investigation Analyzing Effects of Injection Pressure on Efficiency of Matrix Acidizing Stimulation on Marcellus Shale Core Samples. In: 54th U.S. Rock Mechanics/ Geomechanics Symposium. American Rock Mechanics Association. ARMA 20-1294.
8. Dong, B., Meng, M., Qiu, Z., Lu, Z., Zhang, Y., Zhong, H., 2019. Formation damage prevention using microemulsion in tight sandstone gas reservoir. J. Petrol. Sci. Eng. 173, 101-111.
9. Kim, J., Zhang, H., Sun, H., Li, B., Carman, P., 2016. Choosing surfactants for the Eagle Ford shale formation: guidelines for maximizing flowback and initial oil recovery. In: SPE Low Perm Symposium. Society of Petroleum Engineers. SPE-180227-MS.
10. Neog, A., Schechter, D. S., 2016. Investigation of surfactant induced wettability alteration in Wolfcamp shale for hydraulic fracturing and EOR applications. In: SPE Improved Oil Recovery Conference. Society of Petroleum Engineers. SPE-179600-MS.
11. Ahmadi, M., Sharma, M. M., Pope, G., Torres, D. E., McCulley, C. A., Linnemeyer, H., 2011. Chemical treatment to mitigate condensate and water blocking in gas wells in carbonate reservoirs. SPE Prod. Oper. 26 (01), 67-74.
12. Rostami, A., Nasr-El-Din, H. A., 2014. Microemulsion vs. surfactant assisted gas recovery in low permeability formations with water blockage. In: SPE Western North American and Rocky Mountain Joint Meeting. Society of Petroleum Engineers. SPE-169582-MS.
13. Liang, T., Achour, S. H., Longoria, R. A., DiCarlo, D. A., Nguyen, Q. P., 2017. Flow physics of how surfactants can reduce water blocking caused by hydraulic fracturing in low permeability reservoirs. J. Petrol. Sci. Eng. 157, 631-642.
14. Sayed, M., Liang, F., Ow, H., 2018. Novel surface modified nanoparticles for mitigation of condensate and water blockage in gas reservoirs. In: SPE International Conference and Exhibition on Formation Damage Control. Society of Petroleum Engineers. SPE-189959-MS.
15. Paktinat, J., Pinkhouse, J. A., Stoner, W. P., Williams, C., Carder, G. A., Penny, G. S., 2005. Case histories: post-frac fluid recovery improvements of Appalachian Basin gas reservoirs. In: SPE Eastern Regional Meeting. Society of Petroleum Engineers. SPE-97365-MS.
16. Crafton, J. W., Penny, G. S., Borowski, D. M., 2009. Micro-emulsion effectiveness for twenty four wells, Eastern Green River, Wyoming. In: SPE Rocky Mountain Petroleum Technology Conference. Society of Petroleum Engineers. SPE-123280-MS.
17. Penny, G. S., Pursley, J. T., 2007. Field studies of drilling and completion fluids to minimize damage and enhance gas production in unconventional reservoirs. In: European Formation Damage Conference. Society of Petroleum Engineers. SPE-107844-MS.
18. Butler, M., Trueblood, J. B., Pope, G. A., Sharma, M. M., Baran Jr, J. R., Johnson, D., 2009. A field demonstration of a new chemical stimulation treatment for fluid-blocked gas wells. In: SPE Annual Technical Conference and Exhibition. Society of Petroleum Engineers. SPE-125077-MS.
19. Zelenev, A. S., Ellena, L., 2009. Microemulsion technology for improved fluid recovery and enhanced core permeability to gas. In: 8th European Formation Damage Conference. Society of Petroleum Engineers. SPE-122109-MS.
20. CMG, 2019. CMG STARS manual, https://www.cmgl.ca/stars.
21. Khalil, R., Ramezanian, M., Altawati, F., Emadi, H., 2020. Evaluating Pressure and Temperature Effects on Permeability and Elastic Properties of Wolfcamp Formation – An Experimental Study. In: 54th U.S. Rock Mechanics/ Geomechanics

Symposium. American Rock Mechanics Association. ARMA 20-1145.

22. Wijaya, N., Sheng, J. J., 2020. Mitigating near-fracture blockage and enhancing oil recovery in tight reservoirs by adding surfactants in hydraulic fracturing fluid. J. Petrol. Sci. Eng. https://doi.org/10.1016/j.petrol.2019.106611.
23. Wijaya, N., Sheng, J. J. 2020. Optimum surfactant criteria for controlling invasion-induced water blockage in tight water-wet cores. J. Petrol. Sci. Eng. https://doi.org/10.1016/j.petrol.2020.106931.
24. Wijaya, N., Sheng, J. J., 2019. Effect of desiccation on shut-in benefits in removing water blockage in tight water-wet cores. Fuel 244, 314-323. https://doi.org/10.1016/j.fuel.2019.01.180.
25. Khalil, R., Emadi, H., Elwegaa, K., 2019. Investigation of Rock Properties of the Marcellus Formation–An Experimental Study. In: SPE Eastern Regional Meeting. Society of Petroleum Engineers. SPE-196580-MS.
26. Wijaya, N., Sheng, J. J., 2019. Shut-in effect in removing water blockage in shale-oil reservoirs with stress-dependent permeability considered. SPE Reserv. Eval. Eng. https://doi.org/10.2118/195696-PA.
27. Edwards, R. W., Celia, M. A., 2018. Shale gas well, hydraulic fracturing, and formation data to support modeling of gas and water flow in shale formations. Water Resour. Res. 54 (4), 3196-3206.
28. Tangirala, S., Sheng, J. J., 2019. Roles of surfactants during soaking and post leak-off production stages of hydraulic fracturing operation in tight oil-wet rocks. Energ. Fuel. 33(9), 8363-8373.